

Identification of inhibitors of SARS-Cov-2 -S protein and human ACE2 interaction based on secondary metabolites from Rose water: molecular docking approach

Hourieh Kalhor ¹  | Mohaddeseh Taleghani ²  | Ebrahim Honarmand ³ 
Reza Safari ⁴  | Maryam Khayat Kashani ⁵ 

1. Cellular and Molecular Research Center, Qom University of Medical Sciences, Qom, Iran. E-mail: kalhor.h138@yahoo.com
2. Department of Chemistry, Faculty of Science, University of Qom, Qom, Iran. E-mail: faghatbakhodabash@gmail.com
3. Corresponding author, Department of Chemistry, Faculty of Science, University of Qom, Qom, Iran. E-mail: e.honarmand@qom.ac.ir
4. Corresponding author, Department of Chemistry, Faculty of Science, University of Qom, Qom, Iran. E-mail: safari_physicalchemistry@yahoo.com
5. Nutringredientes Research Center, Federal Institute of Education, Science and Technology (IFCE), Brazil. E-Mail: maryamkhayat@yahoo.com

Article Info

Article type:
Research Article

Article history:
Received 7 October 2023
Received in revised form
17 January 2024
Accepted 20 February
2024
Published online 27
March 2024

Keywords:
SARS-CoV-2,
ACE2,
S protein,
molecular docking,
Rosewater.

ABSTRACT

Severe Acute Respiratory Syndrome Coronavirus 2 (SARS-CoV-2) is a new member of the Betacoronavirus family that has led to a pandemic in recent years. It is well documented that the Receptor Binding Domain (RBD) of the S protein (spike glycoprotein) of SARS-CoV-2 binds to the human Angiotensin-Converting Enzyme 2 (ACE2) receptor to enter lower respiratory tract epithelial cells. Thus, inhibition of SARS-CoV-2-RBD/ACE2 interactions presents an interesting research challenge. In this study, molecular docking approaches were applied to identify compounds from Rose water secondary metabolites against SARS-CoV-2. Subsequently, several Rose water secondary metabolites from Rose water were identified, that had the highest percentages of Rosewater, including Eugenol, Alpha-terpineol, Geraniol, Citronellol, Phenylethyl alcohol, Nerol, and Linalool. Autodock vina software was used to perform docking between selected secondary metabolites and the ACE2 binding site of SARS-CoV-2-RBD. The docking results were analyzed based on the binding affinity, binding modes, and physicochemical properties. The results indicated that all selected secondary metabolites could bind to RBD; however, Eugenol had the highest binding affinity (-6.0 kcal/mol) compared to Alpha-terpineol (-5.7 kcal/mol), Geraniol (-5.3 kcal/mol), Phenylethyl alcohol (-5.3 kcal/mol), Citronellol (-4.6 kcal/mol), Nerol (-4.4 kcal/mol), and Linalool (-4.3 kcal/mol). Our Computer Aid Drug Design approach may contribute to the development of new drugs against SARS-CoV-2. However, the effect of these secondary metabolites needs to be evaluated.

Cite this article: Kalhor, H. Taleghani, M. Honarmand, C. Safari, R. & Khayat Kashani, M. (2023). Identification of inhibitors of SARS-Cov-2 -S protein and human ACE2 interaction based on secondary metabolites from Rose water: molecular docking approach, *Advances in Energy and Materials Research*, 1 (1), 1-8. <https://doi.org/10.22091/JAEM.2023.9619.1002>



1. Introduction

The emergence and rapid spread of the novel SARS-CoV-2 virus in early 2020 has caused significant damage to both public health and the economy global [1-3]. It is well documented that this virus belongs to the Coronaviridae family and the Betacoronavirus genera [4]. However, SARS-CoV-2 is an enveloped virus with a ribonucleic acid (RNA) genome that spans approximately 29.8 kilobases in length. At the end of the genome of this virus are four structural proteins: the spike surface protein (S), the envelope protein (E), the membrane protein (M), and the nucleoside protein (N) [5]. Studies have shown that the virus SARS-COV-2 can enter human respiratory epithelial cells via the human angiotensin-converting enzyme 2 (ACE2) receptor, which makes this virus highly transmissible from person to person. It is aproned that the spike protein (S protein) and the main protease (MPro/3Clpro) play crucial roles in the lifecycle of the SARS-COV-2 virus. The S protein facilitates the fusion of the virus with the cell membrane by binding to the ACE2 cell receptor, while the MPro/3Clpro is a crucial enzyme for the replication of the virus; therefore, the S protein and MPro protease may be potential targets for drug design to prevent this virus [6]. Although various approaches; vaccine development, herbal therapies, therapeutic antibody production, etc., have been proposed as possible methods to inhibit and control the spread of this virus, the diseases caused by this virus still pose a great challenge to researchers and clinicians so, they are motivated to introduce and develop potential therapies [7-11]. Since the identification of new drugs by experimental techniques is very time-consuming and costly, it seems logical to search for potential therapeutics by using theoretical methods [11-17]. Thus, in this study, the molecular docking method was used to identify compounds that inhibit the interaction between the S protein of the SARS-Cov-2 virus and human ACE2 protein, using secondary metabolites from Rosewater. Rose water with the scientific name *Rosa damascena* Mill, which belongs to the Rosaceae family and the genus *Roza* [12]. The extract obtained from rosehip contains various compounds such as Eugenol, Quercetin, Kaempferol, and various natural antioxidants. It is believed that this plant may be effective in preventing and even ameliorating certain diseases, including the nervous system, respiratory system, and antiviral diseases [12-15].

In this study, secondary metabolites of Rose water against the RBD domain of SARS-CoV-2 were identified and selected also the binding site of SARS-CoV-2-RBD was selected then molecular docking between selected secondary metabolites was performed. The results showed that among the selected secondary metabolites, Eugenol might be an effective therapeutic

agent for the treatment of SARS-CoV-2 infection owing to its better binding affinities and conformations. The results of this study showed that *in silico* methods can be effectively applied to identify new potential drugs against SARS-CoV-2.

2. Materials and methods

Computer Aid Drug Design (CADD) approaches are increasingly used in drug discovery. Among these, one of the most common CADD techniques are molecular docking and virtual screening. The SBVS method requests the three-dimensional structure of the target protein and identifying binding sites to select ligands that bind strongly to those binding sites [11, 16-18]. In this study, the molecular docking method was used to identify novel SARS-Cov2 inhibitors Rose water secondary metabolites of native Iranian.

2.1. Protein selection and preparation

The X-ray crystal structure of the SARS-CoV-2-RBD/ACE2 complex with PDB entry: 6VW1 was fetched from PDB (<http://www.rcsb.org/pdb>) for molecular docking studies [19]. To prepare the protein, AutoDock Tools 4.2 software was used [20]. The water molecules were removed and atoms were adjusted to the AutoDock atom Types after that bond orders were assigned, as well as hydrogen atoms and Gasteiger-Marsili charges were added to the crystal structure of the protein. Lastly, the structure was ready in the PDBQT format.

2.2. Binding pocket selection and preparation

Based on the data obtained from this crystallography structure (PDB ID: 6VW1), Tyr449, Tyr453, Leu455, Phe456, Ala475, Gly476, Phe486, Asn487, Tyr489, Gln493, Gly496, Gln498, Thr500, Asn501, Gly502 and Tyr505 residues were selected as the binding site for flexible docking. Afterward, AutoDock Tools4.2 software was applied to predict Grid box was into X=26 Å, Y=42 Å, Z=28 Å grid points, and the grid spacing was 1 Å for docking studies.

2.3. Ligand selection and preparation

In the first step, the Rose extract was extracted with traditional techniques; after that, the obtained extract (Rosewater) was analyzed by using GC/Mass (Gas Chromatography Mass spectrometry) method to identify secondary metabolites (**Table 1**).

Table 1. Evaluation of rose water secondary metabolites by GC/Mass method.

| Gas chromatography-mass spectrometry (GC/MS) Analysis | | | | | |
|---|------|------|------------|-----|-------|
| No | RT | % | Components | KI | Type |
| 1 | 8.53 | 0.07 | 1-Hexanol | 873 | Other |

| Gas chromatography-mass spectrometry (GC/MS) Analysis | | | | | |
|---|-------|--------------|----------------------------------|------|-------|
| No | RT | % | Components | KI | Type |
| 2 | 17.20 | 0.52 | Benzyl Alcohol | 1049 | Other |
| 3 | 17.66 | 0.14 | Benzene acetaldehyde | 1058 | Other |
| 4 | 20.17 | 5.30 | Linalool | 1107 | MO |
| 5 | 20.62 | 0.15 | Cis-Rose oxide | 1116 | MO |
| 6 | 21.39 | 41.20 | Phenethyl alcohol | 1132 | Other |
| 7 | 24.01 | 0.06 | ρ - Mentha-1,5-dien-8-ol | 1185 | MO |
| 8 | 24.33 | 0.38 | Terpinen-4-ol | 1191 | MO |
| 9 | 25.13 | 2.29 | α - Terpineol | 1208 | MO |
| 10 | 26.42 | 8.55 | Nerol | 1235 | MO |
| 11 | 26.56 | 13.61 | Citronellol | 1238 | MO |
| 12 | 27.14 | 0.16 | Z-Citral | 1250 | MO |
| 13 | 27.73 | 17.81 | Geraniol | 1263 | MO |
| 14 | 27.98 | 0.35 | β - Phenethyl acetate | 1268 | Other |
| 15 | 28.55 | 0.11 | E-Citral | 1280 | MO |
| 16 | 32.49 | 8.02 | Eugenol | 1367 | Other |
| 17 | 33.26 | 0.12 | Geranyl acetate | 1385 | MO |
| 18 | 34.54 | 0.91 | Methyl eugenol | 1414 | Other |
| 19 | 46.72 | 0.07 | Farnesol | 1725 | SO |
| | | 99.81 | Total Identified | | |
| | | | Monoterpene Hydrocarbons | MH | |
| | | | Oxygenated Monoterpenes | MO | |
| | | | Sesquiterpene Hydrocarbons | SH | |
| | | | Oxygenated Sesquiterpenes | SO | |
| | | | Diterpene Hydrocarbons | DH | |
| | | | Oxygenated Diterpenes | DO | |
| Monoterpene Hydrocarbons | | MH | Oxygenated Monoterpenes | | |
| Sesquiterpene Hydrocarbons | | SH | Oxygenated Sesquiterpenes | | |
| | | MO | | | |
| | | SO | | | |

Subsequently, secondary metabolites with the highest percentage were selected as ligands for molecular docking which included; Eugenol, Alpha-terpineol, Geraniol, Phenylethyl alcohol, Citronellol, Nerol, and Linalool (Figure 1). In the next step, the two-dimensional structure of selected ligands was downloaded from the PubChem database (<https://pubchem.ncbi.nlm.nih.gov>) and saved in SDF format. Subsequently, the 2D structure of ligands was energetically minimized using chem3D (version 17.1) software with Minimize Energy and Molecular Dynamics using MM2 force field [21]. Finally, by using Open Babel software [22], the Optimized ligands were converted to SDF format for molecular docking.

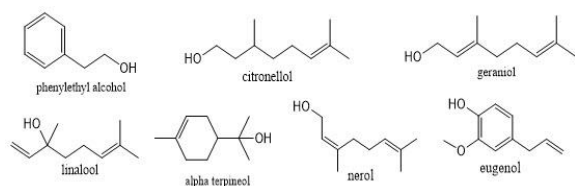


Figure 1. Selected secondary metabolites from Rosewater.

2.4. Molecular Docking Study

In this step, flexible docking was performed using the AutoDock Vina program [23]. Then, the docking results and the molecular interaction between SARS-Cov2-RBD and ligands were evaluated and visualized by using Pymol and LigPlot software [24, 25].

3. Results

3.1. Evaluation of the structure of SARS-CoV-2-S protein and selection of binding site

The evaluation of the primary structure of the S protein of SARS-CoV-2 showed that this protein is encoded by the *s* gene and built of 1273 amino acids with 141.178 Da molecular weight. The S protein sequence from UniProtKB (PODTC2) disclosed that this protein contains a signal peptide from 1 to 13 residues and several domains; N-terminal domain (NTD), receptor binding domain (RBD), subdomain1/2 (SD1/SD2), and S2 domain also this protein includes several disulfide bond and glycosylation sites. It is well documented that the RBD is a key domain of the SARS-CoV-2 S protein which plays an important role in the interaction with human ACE2 enzyme.

Also, the physicochemical properties of the S protein were evaluated using ExPasy's ProtParam (<http://expasy.org/tools/protparam.html>). The computed pI (6.24) of S protein has revealed that this protein has acidic characteristics, and the total number of positively (Arg, Lys) and negatively (Asp, Glu) charged residues are 103 and 110, respectively. Also, the instability index of the S protein is 33.01 proposes that this protein is possibly stable under physiological conditions. The Aliphatic and GRAVY indexes of S protein were 84.67 and -0.07 which showed that this protein is thermostable and hydrophilic, respectively (Table 2).

Table 2. Evaluation of physicochemical properties of S protein of SARS-CoV2 using ProtParam server.

| Protein | Length | MW (D) | pI | -R | +R | GRAVY | Aliphatic Index | Instability Index |
|------------|--------|-----------|------|-----|-----|-------|-----------------|-------------------|
| RBD | 1273 | 141178.47 | 6.24 | 110 | 103 | -0.07 | 84.67 | 33.01 |

MW (D): Molecular weight (Daltons), -R: Negative-charged residues (Asp and Glu), +R: Positive-charged residues (Arg and Lys), GRAVY: Grand average of hydrophaticity

The secondary structure results of S protein by using Vadar software showed that the structure of coil (50%) was the main structure and after β -strands (49%), turn (29%), and α -helix (8%) (Table 3).

Table 3. Evaluation of second structure of S protein from SARS-CoV-2 using Vadar server.

| Protein | Helix % | Beta % | Coil % | Turn % | Mean H-bond distance | Mean H-bond energy | % Residue with H-bonds |
|------------|---------|--------|--------|--------|----------------------|--------------------|------------------------|
| RBD | 8 | 40 | 50 | 29 | 2.2 sd=0.4 | -1.7 sd=1.0 | 65 |

So far, the tertiary structure of the S protein as well as the SARS-CoV2-RBD/ACE2 complex has been extensively studied by using experimental methods. In this study, the crystallographic structure of the SARS-CoV-2-RBD/ACE2 complex with PDB ID: 6VW1 was used to study molecular docking (Figure 2).

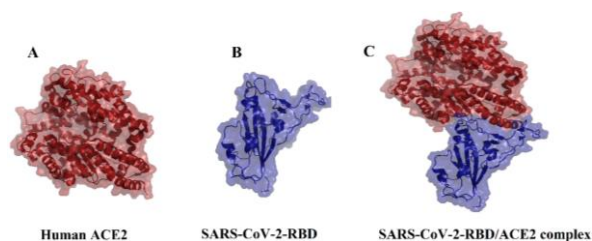


Figure 2. Representation of the structures of Human ACE2 and SARS-CoV2-RBD. Surface representation of (A) Human ACE2, (B) SARS-CoV2-RBD, and (C) SARS-CoV2-RBD/ACE2 complex structures (PDB ID: 6VW1).

In accordance with the previous studies, the ACE2 binding site of SARS-CoV-2 -RBD included residues Tyr449, Tyr453, Lus455, Phe456, Ala475, Gly476, Phe486, Asn487, Tyr489, Gln493, Gly496, Gln498, Thr500, Asn501, Gly502, and Tyr505 were found to be the key residues involved in the SARS-CoV-2-RBD/ACE2 interactions [19]. Taken together, these residues in the C-terminal region of SARS-CoV-2 -RBD were elected as binding sites for further study. Hence, the total charge of proteins was calculated, and the result showed that the total charge SARS-CoV-2 -RBD is 0.000 for 2969 atoms; while the total charge ACE2 is -27.000 for 9505 atoms the result of the total charge SARS-CoV2-RBD/ACE2 complex is -27.000 for 12474 atoms. Also, the evaluation of the electrostatic surface of SARS-CoV-2 -RBD represented that the ACE2 binding site of SARS-CoV-2 -RBD is hydrophobic and about negatively charged (Figure 3). Accordingly, the selected residues as the binding site were hydrophobic and about negatively charged; therefore, they can make a strong electrostatic interaction with the hydrophobic and positively charged secondary metabolites of Rosewater.

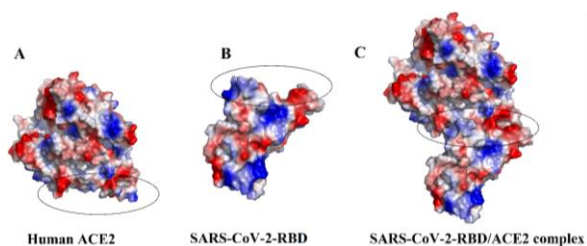


Figure 3. Surface electrostatic potential of Human ACE2 and SARS-CoV2-RBD. Representation of the surface electrostatic potential of (A) Human ACE2 (B) SARS-CoV2-RBD, and (C) SARS-CoV2-RBD/ACE2 complex. Blue: positive regions, red: negative regions, white: hydrophobic. The binding sites of ACE2 and SARS-CoV-2 -RBD are shown in circles.

3.2. Evaluation of binding modes of selected secondary metabolites interactions with SARS-CoV-2 -RBD

The SARS-CoV-2 -RBD complex with selected secondary metabolites was studied in terms of the binding affinity, hydrogen bonds, and interacting residues. The docking results showed that Eugenol had the highest binding affinity (-6.0 kcal/mol) with SARS-

CoV-2-RBD while binding affinity Alpha-terpineol, Phenylethyl alcohol, Geraniol, Citronellol, Nerol, and Linalool compounds were in the range of -4.3 to -5.7 kcal/mol. More details about the binding affinity and interacting residues in the complexes are tabulated in Table 4.

Table 4. Evaluation of the binding affinity (kcal/mol) and interacting residues in the complexes SARS-CoV-2- RBD with selected secondary metabolites.

| Name secondary metabolites | binding affinity (kcal/mol) | HB-Aas ^a | NH-Aas ^b |
|----------------------------|-----------------------------|--------------------------------|--|
| Eugenol | -6.0 | Phe490, Gln493, Phe456 | Leu455 |
| Alpha-terpineol | -5.7 | Phe490, Phe456 | Leu455, Gln493, Leu492, Tyr489 |
| Geraniol | -5.3 | Leu492, Gln493, Phe490 | Leu455 |
| Phenylethyl alcohol | -5.3 | Leu492, Phe456, Gln493 | Leu455, Gln493, Phe490 |
| Citronellol | -4.6 | Leu455, Phe456 | Gln493, Phe490, Pro491 |
| Nerol | -4.4 | Leu492, Gln493, Phe490, Phe456 | Leu455, Tyr489 |
| Linalool | -4.3 | Arg454, Phe456 | Glu471, Lys458, Ser469, Tyr473, Asp467, Arg457 |

^aHydrogen bonds forming Amino Acids, ^bNon-bonded contacts forming Amino Acids

Moreover, hydrogen bonds and hydrophobic interactions between SARS-CoV-2-RBD and selected secondary metabolites were analyzed using the pymol and Ligplot program.

We noticed that the best-scored secondary metabolite, Eugenol, formed three hydrogen bonds and one hydrophobic interaction. The O atoms of Gln493 and Phe490 formed hydrogen bonds with the O atom of the Eugenol with the bond length of 2.67 and 2.91 Å^o, respectively, as well as the C atom of Phe456 with the C atom of the Eugenol formed a hydrogen bond (Figure 4).

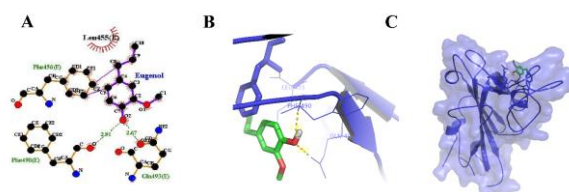


Figure 4. The two-dimensional structure of Eugenol and three-dimensional illustration of its interaction with the ACE2 binding pocket of SARS-CoV-2-RBD. (A) Representation of the 2D structure of Eugenol in the complex. (B) Hydrogen bonds in the protein-ligand complex are shown as yellow dotted lines. (C) 3D illustration of Eugenol (stick representation) in the binding pocket of SARS-CoV-2-RBD (surface representation) (PDB ID: 6vw1).

Alpha-terpineol formed two hydrogen bonds as well as four hydrophobic interactions with the main residues of SARS-CoV-2 -RBD. The O atom of Phe490 with a bond length of 2.81 Å^o and the C atom of Phe456 formed a hydrogen bond (Figure 5).

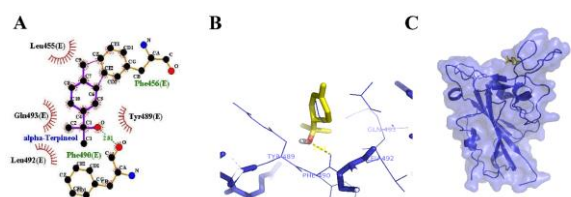


Figure 5. The two-dimensional structure of Alpha-terpineol and three-dimensional illustration of its interaction with the ACE2 binding pocket of SARS-CoV-2-RBD. (A) Representation of 2D structure of Alpha-terpineol in the complex. (B) Hydrogen bonds in the protein-ligand complex are shown as yellow dotted lines. (C) 3D illustration of Alpha-terpineol (stick representation) in the binding pocket of SARS-CoV-2-RBD (surface representation) (PDB ID: 6vw1).

Geraniol formed four hydrogen bonds and one hydrophobic interaction with residues of SARS-CoV-2 -RBD. The O atoms of Phe490, Leu492, and Gln493 with the O atom of Geraniol formed hydrogen bonds with lengths of 2.89, 2.96, and 2.72 Å, respectively, as well as a hydrogen bond between the C atom of Phe456 and C atom Geraniol (Figure 6).

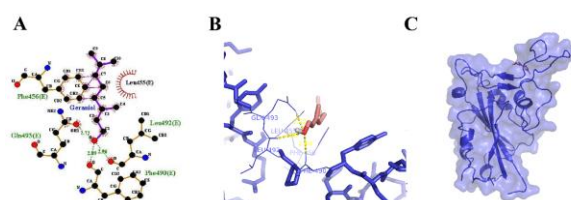


Figure 6. The two-dimensional structure of Geraniol and three-dimensional illustration of its interaction with the ACE2 binding pocket of SARS-CoV-2-RBD. (A) Representation of 2D structure of Geraniol in complex. (B) Hydrogen bonds in the protein-ligand complex are shown as yellow dotted lines. (C) 3D illustration of Geraniol (stick representation) in the binding pocket of SARS-CoV-2-RBD (surface representation) (PDB ID: 6vw1).

In the same manner, Phenylethyl alcohol formed three hydrogen bonds as well as two hydrophobic interactions with important residues of SARS-CoV-2 -RBD. The O atoms of Gln493 and Leu492 formed hydrogen bonds with the O atom of Phenylethyl alcohol with a bond length of 2.87 Å, respectively, and the C atom of Phe456 formed a hydrogen bond with the C atom of Phenylethyl alcohol (Figure 7).

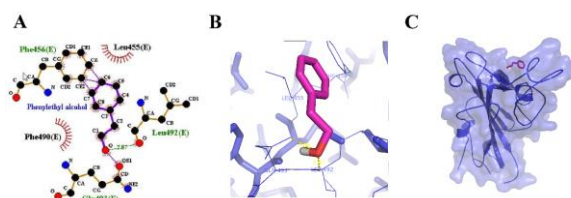


Figure 7. The two-dimensional structure of Phenylethyl alcohol and three-dimensional illustration of its interaction with the ACE2 binding pocket of SARS-CoV-2-RBD. (A) Representation of 2D structure of Phenylethyl alcohol in the complex. (B) Hydrogen bonds in the protein-ligand complex are shown as yellow dotted lines. (C) 3D illustration of Phenylethyl alcohol (stick representation) in the binding pocket of SARS-CoV-2-RBD (surface representation) (PDB ID: 6vw1).

Citronellol formed two hydrogen bonds and three hydrophobic interactions with residues of SARS-CoV-2 -RBD. The O atom of Leu455 with the O atom of

Citronellol formed a hydrogen bond with a length of 2.92 Å and a hydrogen bond between the C atom of Phe456 and the C atom of Citronellol (Figure 8).

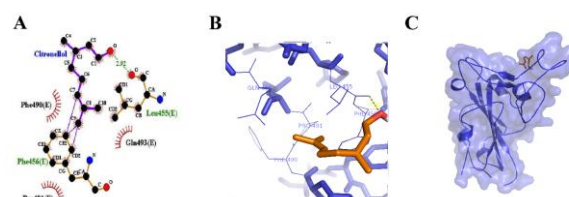


Figure 8. The two-dimensional structure of Citronellol and three-dimensional illustration of its interaction with the ACE2 binding pocket of SARS-CoV-2-RBD. (A) Representation of 2D structure of Citronellol in the complex. (B) Hydrogen bonds in the protein-ligand complex are shown as yellow dotted lines. (C) 3D illustration of Citronellol (stick representation) in the binding pocket of SARS-CoV-2-RBD (surface representation) (PDB ID: 6vw1).

Nerol formed four hydrogen bonds and two hydrophobic interactions with SARS-CoV-2 -RBD. The O atoms of Phe490, Leu492, and Gln493 with the O atom of Nerol formed hydrogen bonds with a length of 2.89, 2.95, and 2.37 Å, in addition to hydrogen bonds between the C atom of Phe456 and C atom Nerol (Figure 9).

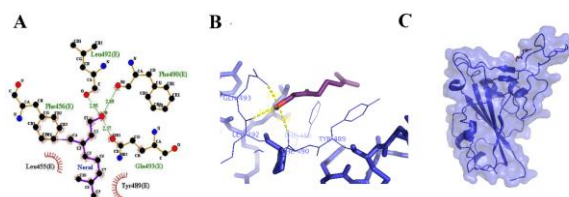


Figure 9. The two-dimensional structure of Nerol and three-dimensional illustration of its interaction with the ACE2 binding pocket of SARS-CoV-2-RBD. (A) Representation of 2D structure of Nerol in the complex. (B) Hydrogen bonds in the protein-ligand complex are shown as yellow dotted lines. (C) 3D illustration of Nerol (stick representation) in the binding pocket of SARS-CoV-2-RBD (surface representation) (PDB ID: 6vw1).

Linalool formed two hydrogen bonds and five hydrophobic bonds with residues of SARS-CoV-2 -RBD. The O atoms of Arg454 and Phe456 with the O atom of Linalool formed hydrogen bonds with lengths of 3.02 and 2.71 Å, respectively (Figure 10).

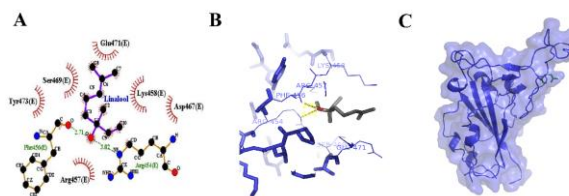


Figure 10. The two-dimensional structure of Linalool and three-dimensional illustration of its interaction with the ACE2 binding pocket of SARS-CoV-2-RBD. (A) Representation of 2D structure of Linalool in the complex. (B) Hydrogen bonds in the protein-ligand complex are shown as yellow dotted lines. (C) 3D illustration of Linalool (stick representation) in the binding pocket of SARS-CoV-2-RBD (surface representation) (PDB ID: 6vw1).

4. Discussion

It is well documented that the RBD domain of the SARS-CoV-2 S protein binds to human ACE2.

Interestingly, this binding mechanism is similar to that of SARS-CoV [26]. Also, the previous study of the superimposition of SARS-CoV-2-RBD and SARS-CoV-RBD complexes with ACE2 reported that the residues of SARS-CoV-2-RBD involved in the interaction with ACE2, Tyr449, Tyr453, Asn487, Tyr489, Gly496, Thr500, Gly502 and Tyr505 residues, were identical to the ACE2-binding site of SARS-CoV [11]. Hence, the binding site of SARS-CoV-2-RBD to ACE2 could be an important target for drug discovery. In this regard, using AutoDock Vina software, molecular docking was done between flexible residues of the selected binding site of SARS-CoV-2-RBD, Tyr449, Tyr453, Lys455, Phe456, Ala475, Gly476, Phe486, Asn487, Tyr489, Gln493, Gly496, Gln498, Thr500, Asn501, Gly502, and Tyr505 residues, and selected secondary metabolites from Rosewater, Eugenol (PubChem CID: 3314), Alpha-terpineol (PubChem CID: 17100), Geraniol (PubChem CID: 637566), Phenylethyl alcohol (PubChem CID: 6054), Citronellol (PubChem CID: 8842), Nerol (PubChem CID: 643820), and Linalool (PubChem CID: 6549). Afterward, the molecular docking results were analyzed based on the binding affinity. The molecular docking results showed that the binding affinity of Eugenol (-6.0 kcal/mol) was better than that of other selected secondary metabolites (Table 4).

Also, the analysis of the interaction of the secondary metabolites with RBD, displayed that Eugenol had better conformation compared to other metabolites (Figures 5-10).

It is well documented that most orally active follow Lipinski's Rule of fFve (RO5) which includes the following; molecular weight < 500 Da, Xlogp (octanol-water partition coefficient) < 5, H-bond acceptor < 10 and H-bond donors < 5 [27]. To investigate RO5, key pharmacokinetic properties of the secondary metabolites of Rosewater were investigated using the PubChem database. The results showed that all compounds possessed the following physicochemical properties: MW < 165, cLogP < 3.2, HBD < 2, HBA < 2, PSA < 30 Å², and RB < 5, which are summarized in Table 3.

However, Eugenol had the highest molecular weight, the highest number of H-bond acceptors, and the largest Polar surface area than other compounds. Interestingly that the physicochemical properties of Alpha-terpineol, Geraniol, Citronellol, Nerol, and Linalool compounds were similar. As can be deduced from Table 5, Phenylethyl alcohol had the lowest molecular weight but the other physicochemical properties were similar to other compounds. Therefore, selected secondary metabolites of Rose water possessed RO5.

Eugenol (4-allyl-2-methoxyphenol) is an aromatic compound belonging to the group of phenylpropanoids. Commonly, there is Eugenol in the natural essential oils of plants [28, 29] interestingly, the US Food and Drug

Administration (FDA) is proven that it is a compound non-mutagenic and non-carcinogenic [30]. Also, Eugenol has various pharmacological activities; however, the most important activities include; anticancer [31-33], antioxidant [34-36], antimicrobial [37-39], and anti-inflammatory [40, 41].

It is necessary to mention that, not only Eugenol has low chemical stability but also it is sensitive to oxidation. therefore, if orally administered, it rapidly will be absorbed by different organs and metabolized in the liver. As a result, Eugenol should be encapsulation to prevent early absorption also improve its water solubility and increase its activity [29, 37]. It appears that selected secondary metabolites of Rosewater, spatially Eugenol, had favorable interactions with SARS-CoV-2-RBD; therefore, these compounds could be candida compounds for experimental surveys in limiting SARS-CoV-2-RBD /ACE2 interactions.

Table 5. Evaluation of physicochemical properties of Secondary metabolites using PubChem database.

| Name Secondary metabolites | Physicochemical properties | | | | | | | |
|----------------------------------|----------------------------|-----------------|-----------------|------------------|------------------|------------------|------------------|-----------------|
| | PubID ^a | MF ^b | MW ^c | CLP ^d | HBA ^e | HBD ^f | PSA ^g | RB ^h |
| Eugenol | 3314 | C10H12O2 | 164.20 | 2 | 2 | 1 | 29.5 | 3 |
| Alpha-terpineol | 17100 | C10H18O | 154.25 | 1.8 | 1 | 1 | 20.2 | 1 |
| Geraniol | 637566 | C10H18O | 154.25 | 2.9 | 1 | 1 | 20.2 | 4 |
| Phenylethyl alcohol | 6054 | C6H5CH2CH2OH | 122.16 | 1.4 | 1 | 1 | 20.2 | 2 |
| Citronellol | 8842 | C10H20O | 156.26 | 3.2 | 1 | 1 | 20.2 | 5 |
| Nerol | 643820 | C10H18O | 154.25 | 2.9 | 1 | 1 | 20.2 | 4 |
| Linalool | 6549 | C10H18O | 154.25 | 2.7 | 1 | 1 | 20.2 | 4 |

^aPubChemCID ^bMolecularFormula ^cMolecular weight (g/mol), ^dcLogP(lipophilicity), ^eH-bond acceptors, ^fH-bond donors, ^gPolar Surface Area(Å²), ^hRotatable bonds.

5. Conclusion:

The RBD domain of the SARS-CoV-2-S protein is a crucial domain in binding to the ACE2 receptor; therefore, inhibiting SARS-CoV-2 -S protein and human ACE2 interaction need to be studied. The results of docking and molecular interactions between SARS-CoV-2-RBD and selected secondary metabolites of Rose water demonstrated that Eugenol has better binding affinity and conformation compared to Alpha-terpineol, Geraniol, Citronellol, Phenylethyl alcohol, Nerol, and Linalool. In addition, the evaluation of physicochemical properties showed that all compounds possessed RO5. However, the efficiency of the selected secondary metabolites requests to survey *in vitro* and *in vivo* as well as the obtained results can provide data for the next studies.

Disclosure statement

No potential conflict of interest was reported by the authors.

Funding

This study has been supported by University of Qom (Iran).

REFERENCES

1. Nicola, M., et al., *The socio-economic implications of the coronavirus pandemic (COVID-19): A review*. International journal of surgery, 2020. 78: p. 185-193. DOI: <https://doi.org/10.1016/j.ijssu.2020.04.018>.
2. Huang, C., et al., *Clinical features of patients infected with 2019 novel coronavirus in Wuhan, China*. The lancet, 2020. 395(10223): p. 497-506. DOI: [https://doi.org/10.1016/S0140-6736\(20\)30183-5](https://doi.org/10.1016/S0140-6736(20)30183-5).
3. Chen, N., et al., *Epidemiological and clinical characteristics of 99 cases of 2019 novel coronavirus pneumonia in Wuhan, China: a descriptive study*. The lancet, 2020. 395(10223): p. 507-513. DOI: [https://doi.org/10.1016/S0140-6736\(20\)30211-7](https://doi.org/10.1016/S0140-6736(20)30211-7).
4. Tavakoli, A., K. Vahdat, and M. Keshavarz, *Novel coronavirus disease 2019 (COVID-19): an emerging infectious disease in the 21st century*. ISMJ, 2020. 22(6): p. 432-450. DOI: <https://doi.org/10.29252/ismj.22.6.432>.
5. Wu, C., et al., *Analysis of therapeutic targets for SARS-CoV-2 and discovery of potential drugs by computational methods*. Acta Pharmaceutica Sinica B, 2020. 10(5): p. 766-788. DOI: <https://doi.org/10.1016/j.apsb.2020.02.008>.
6. Khaerunnisa, S., et al., *Potential inhibitor of COVID-19 main protease (Mpro) from several medicinal plant compounds by molecular docking study*. Preprints, 2020. 2020: p. 2020030226. DOI: <https://doi.org/10.20944/preprints202003.0226.v1>.
7. Iacob, S. and D.G. Iacob, *SARS-coV-2 treatment approaches: numerous options, no certainty for a versatile virus*. Frontiers in Pharmacology, 2020. 11: p. 1224. DOI:10.3389/fphar.2020.01224. DOI: <https://doi.org/10.2217/fvl-2020-0137>.
8. Rehman, M., et al., *Therapeutic and vaccine strategies against SARS-CoV-2: past, present and future*. Future Virology, 2020. 15(7): p. 471-482. DOI: <https://doi.org/10.2217/fvl-2020-0137>.
9. Niknam, Z., et al., *Potential therapeutic options for COVID-19: an update on current evidence*. European journal of medical research, 2022. 27: p. 1-15. DOI: <https://doi.org/10.1186/s40001-021-00626-3>.
10. Khan, T., et al., *Therapeutic potential of medicinal plants against COVID-19: The role of antiviral medicinal metabolites*. Biocatalysis and agricultural biotechnology, 2021. 31: p. 101890. DOI: <https://doi.org/10.1016/j.bcab.2020.101890>.
11. Kalhor, H., et al., *Repurposing of the approved small molecule drugs in order to inhibit SARS-CoV-2 S protein and human ACE2 interaction through virtual screening approaches*. Journal of Biomolecular Structure and Dynamics, 2022. 40(3): p. 1299-1315. DOI: <https://doi.org/10.1080/07391102.2020.1824816>.
12. Rezaee, M., et al., *Comparative study of laboratory and industrial essential oils samples of Rosa damascena Mill. for quantitative and qualitative constituents from Kashan*. Iranian Journal of Medicinal and Aromatic Plants Research, 2003. 19(1): p. 63-72. DOI: <https://doi.org/20.1001.1.16807073.2019.21.2.7.8>.
13. Beheshti, F., et al., *A mini review of neuropharmacological effects of Rosa damascena Herm*. Pharmaceutical Sciences, 2021. 28(2): p. 232-238. DOI: <https://doi.org/10.34172/PS.2021.49>.
14. Nikbakht, A. and M. Kafi. *A study on the relationships between Iranian people and Damask rose (Rosa damascena) and its therapeutic and healing properties*. in VIII International People-Plant Symposium on Exploring Therapeutic Powers of Flowers, Greenery and Nature 790. 2004. DOI: <https://doi.org/10.17660/ActaHortic.2008.790.36>.
15. Boskabady, M.H., et al., *Pharmacological effects of Rosa damascena*. Iranian journal of basic medical sciences, 2011. 14(4): p. 295. DOI: <https://doi.org/10.22038/ijbms.2011.5018>.
16. Kalhor, H., et al., *Identification of new DNA gyrase inhibitors based on bioactive compounds from streptomyces: Structure-based virtual screening and molecular dynamics simulations approaches*. Journal of Biomolecular Structure and Dynamics, 2020. 38(3): p. 791-806. DOI: <https://doi.org/10.1080/07391102.2019.1588784>.
17. Kalhor, H., et al., *Novel small molecules against two binding sites of Wnt2 protein as potential drug candidates for colorectal cancer: A structure based virtual screening approach*. Iranian journal of pharmaceutical research: IJPR, 2020. 19(2): p. 160. DOI: <https://doi.org/10.22037/ijpr.2019.15297.13037>.
18. Kalhor, H., et al., *Interactions of heparin derivatives with recombinant human keratinocyte growth factor: Structural stability and bioactivity effect study*. Proteins: Structure, Function, and Bioinformatics, 2023. 91(4): p. 542-554. DOI: <https://doi.org/10.1002/prot.26448>.
19. Shang, J., et al., *Structural basis of receptor recognition by SARS-CoV-2*. Nature, 2020. 581(7807): p. 221-224. DOI: <https://doi.org/10.1038/s41586-020-2179-y>.
20. Morris, G.M., et al., *AutoDock4 and AutoDockTools4: Automated docking with selective receptor flexibility*. Journal of computational chemistry, 2009. 30(16): p. 2785-2791. DOI: <https://doi.org/10.1002/jcc.21256>.
21. *Semiempirical Methods, in Computational Chemistry and Molecular Modeling: Principles and Applications*. 2008, Springer Berlin Heidelberg: Berlin, Heidelberg. p. 139-154. DOI: <https://doi.org/10.1007/978-3-540-77304-7>.
22. O'Boyle, N.M., et al., *Open Babel: An open chemical toolbox*. Journal of cheminformatics, 2011. 3(1): p. 1-14. DOI: 10.1186/1758-2946-3-33. DOI: <https://doi.org/10.1186/1758-2946-3-33>.
23. Trott, O. and A.J. Olson, *AutoDock Vina: improving the speed and accuracy of docking with a new scoring function, efficient optimization, and multithreading*. J Comput Chem, 2010. 31(2): p. 455-461. DOI: <https://doi.org/10.1002/jcc.21334>.

24. DeLano, W. L. (2002). The PyMOL molecular graphics system to bedside: Structure-based drug design on protein targets. *Current Pharmaceutical Design*, 18(9), 1217–1239. doi: <https://doi.org/10.3390/molecules200713384>.
25. Laskowski, R.A. and M.B. Swindells, *LigPlot+ : multiple ligand–protein interaction diagrams for drug discovery*, 2011, ACS Publications. DOI: <https://doi.org/10.1021/ci200227u>.
26. Rismanbaf, A., *Potential treatments for COVID-19; a narrative literature review*. *Archives of academic emergency medicine*, 2020. 8(1). DOI: <https://doi.org/10.22037/aaem.v8i1.596>.
27. Lipinski, C.A., et al., *Experimental and computational approaches to estimate solubility and permeability in drug discovery and development settings*. *Advanced drug delivery reviews*, 2012. 64: p. 4-17. DOI: [https://doi.org/10.1016/s0169-409x\(00\)00129-0](https://doi.org/10.1016/s0169-409x(00)00129-0).
28. Nisar, M.F., et al., *Pharmacological properties and health benefits of eugenol: A comprehensive review*. *Oxidative Medicine and Cellular Longevity*, 2021. 2021. DOI: <https://doi.org/10.1155/2021/2497354>.
29. Ulanowska, M. and B. Olas, *Biological properties and prospects for the application of eugenol—a review*. *International Journal of Molecular Sciences*, 2021. 22(7): p. 3671. DOI: <https://doi.org/10.3390/ijms22073671>.
30. Bendre, R.S., et al., *Outlooks on medicinal properties of eugenol and its synthetic derivatives*. *Nat Prod Chem Res*, 2016. 4(3): p. 1-6. DOI: <https://doi.org/10.4172/2329-6836.1000212>.
31. Hussain, A., et al., *Eugenol enhances the chemotherapeutic potential of gemcitabine and induces anticarcinogenic and anti-inflammatory activity in human cervical cancer cells*. *Cancer Biotherapy and Radiopharmaceuticals*, 2011. 26(5): p. 519-527. DOI: <https://doi.org/10.1089/cbr.2010.0925>.
32. Kaur, G., M. Athar, and M.S. Alam, *Eugenol precludes cutaneous chemical carcinogenesis in mouse by preventing oxidative stress and inflammation and by inducing apoptosis*. *Molecular Carcinogenesis*: Published in cooperation with the University of Texas MD Anderson Cancer Center, 2010. 49(3): p. 290-301. DOI: <https://doi.org/10.1002/mc.20601>.
33. Okada, N., et al., *Induction of cytotoxicity and apoptosis and inhibition of cyclooxygenase-2 gene expression by eugenol-related compounds*. *Anticancer Research*, 2005. 25(5): p. 3263-3269. PMID: 16101137.
34. Tammannavar, P., et al., *An unexpected positive hypersensitive reaction to eugenol*. *Case Reports*, 2013. 2013: p. bcr2013009464. DOI: <https://doi.org/10.1136/bcr-2013-009464>.
35. Gülçin, İ., *Antioxidant activity of eugenol: A structure–activity relationship study*. *Journal of medicinal food*, 2011. 14(9): p. 975-985. DOI: <https://doi.org/10.1089/jmf.2010.0197>.
36. Nam, H. and M.-M. Kim, *Eugenol with antioxidant activity inhibits MMP-9 related to metastasis in human fibrosarcoma cells*. *Food and chemical toxicology*, 2013. 55: p. 106-112. DOI: <https://doi.org/10.1016/j.fct.2012.12.050>.
37. Marchese, A., et al., *Antimicrobial activity of eugenol and essential oils containing eugenol: A mechanistic viewpoint*. *Critical reviews in microbiology*, 2017. 43(6): p. 668-689. DOI: <https://doi.org/10.1080/1040841X.2017.1295225>.
38. Devi, K.P., et al., *Eugenol (an essential oil of clove) acts as an antibacterial agent against Salmonella typhi by disrupting the cellular membrane*. *Journal of ethnopharmacology*, 2010. 130(1): p. 107-115. DOI: <https://doi.org/10.1016/j.jep.2010.04.025>.
39. Gill, A. and R. Holley, *Inhibition of membrane bound ATPases of Escherichia coli and Listeria monocytogenes by plant oil aromatics*. *International journal of food microbiology*, 2006. 111(2): p. 170-174. DOI: <https://doi.org/10.1016/j.jfoodmicro.2006.04.046>.
40. Barboza, J.N., et al., *An overview on the anti-inflammatory potential and antioxidant profile of eugenol*. *Oxidative medicine and cellular longevity*, 2018. 2018. DOI: <https://doi.org/10.1155/2018/3957262>.
41. Magalhães, C.B., et al., *In vivo anti-inflammatory action of eugenol on lipopolysaccharide-induced lung injury*. *Journal of Applied Physiology*, 2010. 108(4): p. 845-851. DOI: <https://doi.org/10.1152/jappphysiol.00560.2009>.